



Effect of sintering temperature on magnetization and Mössbauer parameters of cobalt ferrite nanoparticles



Grish Chandra^{a,*}, R.C. Srivastava^b, V.R. Reddy^c, H.M. Agrawal^b

^a Department of Physics, DSB Campus Kumaun University, Nainital 263002, Uttarakhand, India

^b Department of Physics, GB Pant University of Agriculture and Technology, Pantnagar, Uttarakhand, India

^c UGC-DAE CSR, Khandua Road, DAVV Campus, Indore 452017, Madhya Pradesh, India

ARTICLE INFO

Keywords:

VSM
TEM
XRD
Coercivity
Remanence
Hysteresis

ABSTRACT

Nanoparticles of cobalt ferrite of different particle size were prepared using sol-gel method. Powder X-ray diffraction (XRD), transmission electron microscopy (TEM), vibrating sample magnetometer (VSM) and Mössbauer spectroscopy techniques were employed for characterization of nanoparticles for structural and magnetic properties. The particle size and saturation magnetization increase with the increase of sintering temperature. The saturation magnetization increases from 53 to 85 emu/g as the sintering temperature increases from 300 to 900 °C. The remanence increases while the coercivity decreases slightly with the increase of sintering temperature. Mössbauer spectra show the ferrimagnetic nature of all the samples and the cation distribution strictly depends on the sintering temperature. The stoichiometry of the cobalt ferrite formed was estimated to be $(\text{Co}^{2+}_x\text{Fe}^{3+}_{1-x})[\text{Co}^{2+}_{1-x}\text{Fe}^{3+}_{1+x}]_4\text{O}_4$, based on our Mössbauer analysis. The inverse spinel structure gradually transforms towards the normal spinel structure as the sintering temperature increases.

1. Introduction

Nanomaterials based on ferrites have already a large number of applications, including photocatalysis, adsorption technologies, gas sensors, microwave devices and others [1,2]. Nanosized ferrites have been studied extensively in recent years because of their unusual properties such as high Curie temperature, large magnetocrystalline anisotropy, moderate saturation magnetization, excellent chemical stability and mechanical hardness. The magnetic properties of these nanoparticles are governed by single domain magnetic structure and exhibit unique phenomenon such as superparamagnetism and quantum tunneling of magnetization [2]. Ferrimagnetic cubic spinels, with the combined properties of magnetic materials and insulators are found to be important in technological applications such as in high density information storage, ferrofluids technology, magnetocaloric refrigeration, magnetic resonance imaging (MRI) enhancement, magnetically guided drug delivery and many other biomedical applications etc. [3,4]. The electrical, magnetic and optical properties of these ferrites depend on the magnetic interactions and cation distribution in the two sub lattices i.e. tetrahedral (A) and octahedral (B) sites. Therefore, the control of cationic occupancies at the interstices is very important in order to regulate the magnetic properties of the nanoparticles [4]. Various preparation techniques, such as sol-gel methods,

citrate precursor techniques [5], electrochemical synthesis [6], combustion methods [7], solid state reaction [8], and mechanical alloying [9] are commonly used to prepare ferrite nanoparticles.

Cobalt ferrite is a hard magnetic material that has a high coercivity (~ kOe), high magnetocrystalline anisotropy and large saturation magnetization. Recently cobalt ferrite has attracted considerable attention due to their large magnetostrictive coefficient, chemical stability and mechanical hardness [10]. In bulk form CoFe_2O_4 is a partially inverse spinel structure represented as $(\text{Co}_x\text{Fe}_{1-x})[\text{Co}_{1-x}\text{Fe}_{1+x}]_4\text{O}_4$, where x depends on thermal history and preparation condition [11,12]. Round and square brackets indicate A and B sites respectively. It is ferrimagnetic in nature at room temperature having Curie temperature ~520 °C [13]. In the present work the dependency of cation distribution, between A and B sites, with sintering temperature were studied and the structural and magnetic properties of the cobalt ferrite have also been discussed.

2. Experimental

Sol gel technique was used for the preparation of cobalt ferrite [14,15]. The stoichiometric amounts of $\text{Fe}(\text{NO}_3)_3 \cdot 9\text{H}_2\text{O}$, $\text{Co}(\text{NO}_3)_2 \cdot 6\text{H}_2\text{O}$ and $\text{Ce}(\text{NO}_3)_3 \cdot 6\text{H}_2\text{O}$ were dissolved in distilled water. In the aqueous salt solution, citric acid solution was added with the cations to

* Corresponding author.

E-mail address: grishphysics@gmail.com (G. Chandra).

citric acid molar ratio of 1:3. The solution was heated at 80 °C under constant magnetic stirring until the solution got converted into a viscous gel, and was allowed to cool at room temperature. The cooled gel was dried in a furnace at 100 °C for overnight to form the precursor material. The precursor material was sintered at four different temperatures 300, 500, 700 and 900 °C for 2 h and furnace cooled to room temperature to get the nanoparticles of cobalt ferrite having different particle size. X-ray diffraction data were collected by using Bruker D8 ADVANDED X-ray diffractometer having Cu K α radiation ($\lambda=1.54178$ Å). High-field magnetization measurements at room temperature were carried out with the help of a Quantum Design Vibrating Sample Magnetometer (VSM, Model 6000 Physical Property Measurement System). Mössbauer spectroscopy measurements were performed using a conventional constant acceleration Mössbauer spectrometer in transmission geometry. The source was a ^{57}Co source in Rh matrix with strength 25 mCi. The isomer shift and velocity scale were calibrated with respect to a $\alpha\text{-Fe}$ foil at room temperature.

3. Result and discussion

3.1. Structural characterization

Fig. 1 shows the XRD patterns of the cobalt ferrite nanoparticles prepared by sol-gel technique and sintered at different temperatures. The diffraction peaks are corresponding to the single phase of the ferrite nanoparticles and having no impurity peaks. The phase analysis was done with JCPDS (Joint Committee on Powder Diffraction Standards) card number 03–0864. The crystallite size is determined by Scherrer formula [16] using the most intense peak (311)

$$D = \frac{k\lambda}{\beta \cos\theta}$$

where λ is the wavelength of X-ray used, θ is the Bragg's angle, β is the full width at half maximum (FWHM) in radian and ' k ' is a constant approximately equal to 0.9 [14–16]. As the sintering temperature increases, the XRD peaks become sharper which shows an increase in the crystallite size of the sample. The crystallite size of the samples sintered at 300, 500, 700 and 900 °C are 10, 21, 34 and 40 nm respectively. The crystallite size increases significantly when the sintering temperature exceeds 500 °C [6]. The lattice parameter was calculated with the help of the relation:

$$a = d_{hkl}(h^2 + k^2 + l^2)^{1/2}$$

where h, k, l are the Miller indices of the planes having interplanar spacing ' d '. All the parameters obtained from the XRD patterns are

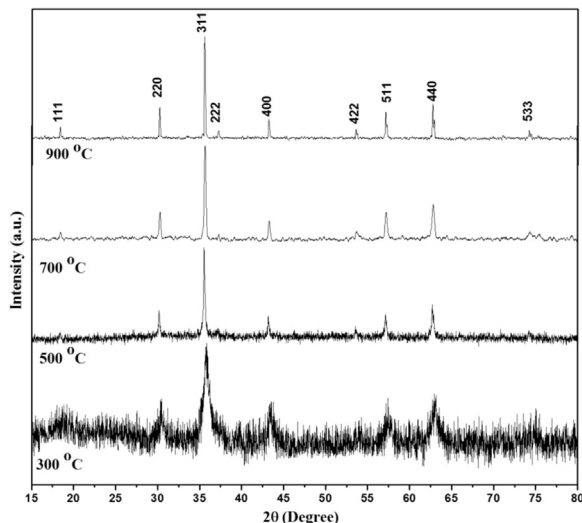


Fig. 1. XRD patterns of CoFe_2O_4 sintered at different temperatures.

Table 1

XRD parameters for synthesized samples.

Sintering temp. (°C)	Particle size (± 2 nm)	Lattice parameter (± 0.002 Å)
300	10	8.341
500	21	8.385
700	34	8.382
900	40	8.384

listed in Table 1.

For the direct observation of the particle size the transmission electron microscopy was used. A typical TEM image is shown in Fig. 2a for the CoFe_2O_4 sample sintered at 500 °C. The selected area diffraction (SAD) pattern is also shown in the inset of the TEM image and it indicates the pure spinel phase and crystalline nature of CoFe_2O_4 . The rings correspond to the reflections from (111), (220), (311) and (400) planes [4–18]. These planes are the characteristics of spinel phase of the sample. A histogram of the particle size distribution is shown in Fig. 2b. The average particle size calculated with Lorentz fitting, is of the order of 25 nm, which confirms the XRD results. These particles are smaller than the critical domain size (~ 40 nm) [20] for cobalt ferrite. The particles observed in TEM image should be single domain in size. The distribution seems to be symmetric about 25 nm size. Most of the particles appear spherical in shape however some elongated particles are also present as shown in the TEM image. Some agglomerated particles as well as separated particles are present in the image. Ring shape of selected area electron diffraction pattern confirms formation of CoFe_2O_4 nanocrystals.

3.2. VSM study

The hysteresis loops of the CoFe_2O_4 sintered at various temperatures are shown in Fig. 3. No saturation is observed under the maximum applied field of ± 3 T. The saturation magnetization was calculated by fitting the high field magnetization data using the relation [21,22]

$$M = M_s(1 - a/H)$$

where M_s is the saturation magnetization, ' a ' is the fitting parameter and H is applied external magnetic field. Using above relation the specific magnetization measured at room temperature and at high field strength varies almost linearly with $1/H$. The saturation magnetization is estimated from the intercept with the magnetization axis as $1/H$ approaches to zero [6]. A curve for the variation of saturation magnetization, remanence and coercivity with particle size is shown in Fig. 4.

In the ideal situation when the prepared sample grows into pure inverse spinel crystal structure, with all the Co^{+2} ions located at the octahedral site, the magnetization per formula unit can be calculated by the difference between the magnetization of A and B sites, i.e., $M = M_B - M_A$. The magnetic moment of Fe^{+3} and Co^{+2} cations are 5.0 and $3.8 \mu_B$ respectively [23,24], a theoretical magnetic moment of CoFe_2O_4 is $3.0 \mu_B$ per formula unit (at 0 K). In our study the magnetic moment per formula unit (f.u.) is varying from 2.21 to $3.57 \mu_B$ as the sintering temperature is varying from 300 to 900 °C. The result $3.57 \mu_B/\text{f.u.}$ is consistent with the theoretical value of $3.60 \mu_B/\text{f.u.}$ calculated by Slonczewski [25] in which they assumed that the structure of cobalt is not completely inverse spinel and the degree of the inversion depends on the heat treatment.

It is clear that the value of saturation magnetization is increased by increasing the sintering temperature. This result can be attributed to the nanosized cobalt ferrite particles in which the surface areas are larger and thus the surface energy is high. Moreover; the variation of saturation magnetization with heat treatment is possibly due to change in the degree of inversion in CoFe_2O_4 in which the exchange of Fe^{+3}

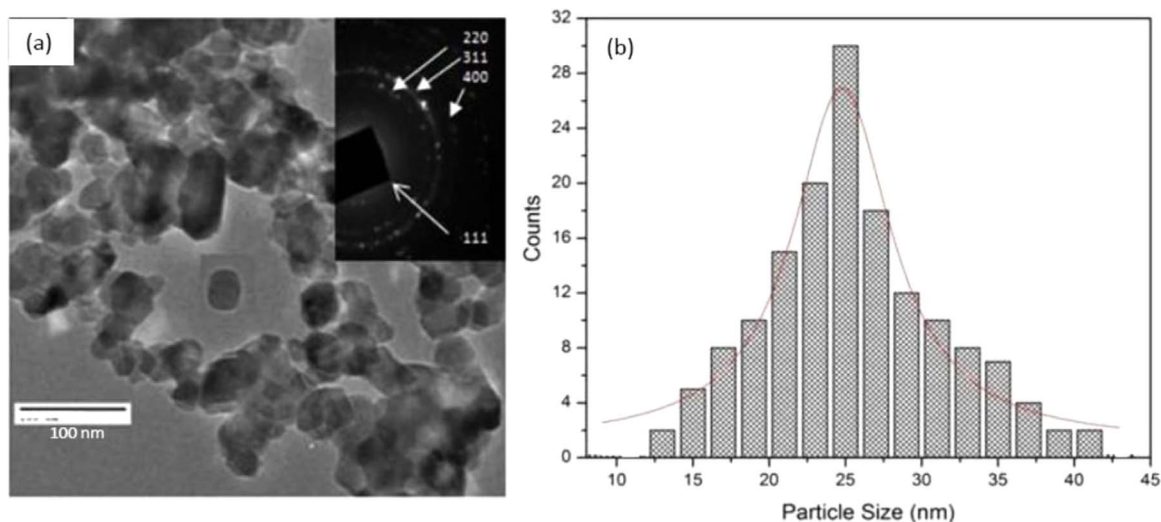


Fig. 2. (a) Transmission electron micrograph (inset shows SAD of same sample), (b) histogram of particle size distribution (red line shows Lorentz fit) for the sample sintered at 500 °C. (For interpretation of the references to color in this figure legend, the reader is referred to the web version of this article.)

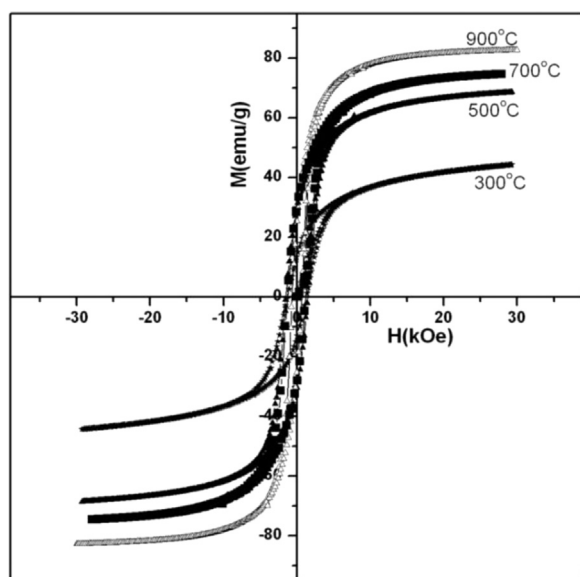


Fig. 3. *M* vs. *H* curve for cobalt ferrite sintered at four different temperatures.

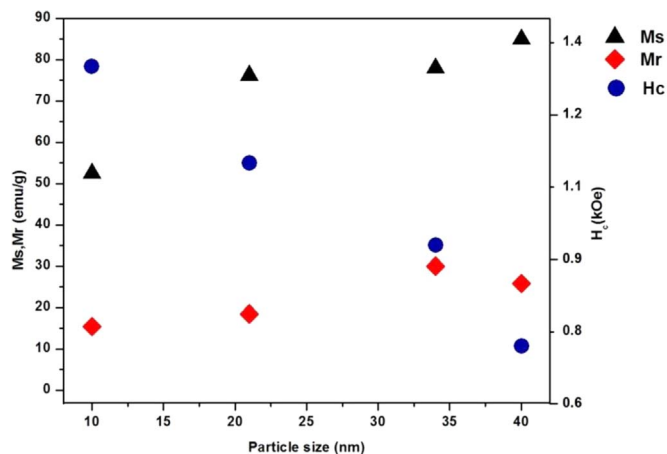


Fig. 4. Variation of *M_s*, *M_r* and *H_c* with particle size..

and Co^{+2} cations from A and B site and vice versa. The saturation magnetization of the annealed sample at 900 °C is ~85 emu/g. Singhal et al. [14] found the saturation magnetization value (84.5 emu/g) of same composition prepared by aerosol route after sintering at 1000 °C. The magnetic moment per formula unit (magneton number n_B) can be calculated from the hysteresis loops at room temperature from the following relation [22–25]

$$n_B = \frac{\text{molecular weight} \times \text{saturation magnetization (emu/g)}}{5585} \mu_B$$

The values of magneton numbers are given in Table 2. The coercivity for these samples were found to decrease from 1.3 to 0.72 kOe while magnetic moments were found to increase from 52 to 85 emu/g for these samples as the sintering temperature increases from 300 to 900 °C. It is clear from the Table 2 that the magnetic parameters are highly dependent on the sintering temperature of the sample. It should be noted that the single domain size of cobalt ferrite material is estimated to be ~40 nm. The smaller value of saturation magnetization for the sample sintered at 300 °C is attributed to the superparamagnetic nature of the particles [26]. The variation of H_c is different from M_s and M_r , which indicates that the particle size of cobalt ferrite is not the unique factor for determining H_c . It is closely related to the microstructure, particle size and residual strain etc. The decrease in H_c for the sample sintered at 900 °C may be due to the transition from magnetic single domain to the magnetic multi domain within a particle and decrease in anisotropy field. In general the coercive field H_c increases as the particle size increases (within the single domain region) [26]. However, a decrease in H_c is observed with the increase in particle size. This kind of behavior was also observed in similar systems by previous workers [27]. Therefore a deeper investigation of the observed behavior of H_c is desired.

3.3. Mössbauer study

The room temperature Mössbauer spectra of cobalt ferrite samples sintered at four different temperatures are shown in Fig. 5. It contains two sextets which signify the ferrimagnetic nature of the samples. One sextet corresponds to the tetrahedral (A-site) site and another corresponds to the octahedral (B-site) site. Outer sextet corresponding to the tetrahedral A-site and inner sextet corresponding to the octahedral B-site. To extract the hyperfine magnetic field distribution, the standard least square fitting program (SITE) NORMOS was applied [28]. From the area ratio $r = A_A/A_B$ of the subspectra A and B the parameter, $x = (1-r)/(1+r)$ can be calculated (assuming that recoil free fraction at room

Table 2
Magnetic parameters for the cobalt ferrite sample sintered at different temperatures.

Sintering temp. (°C)	Saturation Magnetization (± 0.05 emu/g)	Remanence (± 0.05 emu/g)	Coercivity (± 0.02 kOe)	Magneton number (μ_B)
300	52.53	15.39	1.30	2.21
500	76.23	18.45	1.1	3.20
700	78.03	30.03	0.93	3.28
900	84.97	25.86	0.72	3.57

n_B = magneton number.

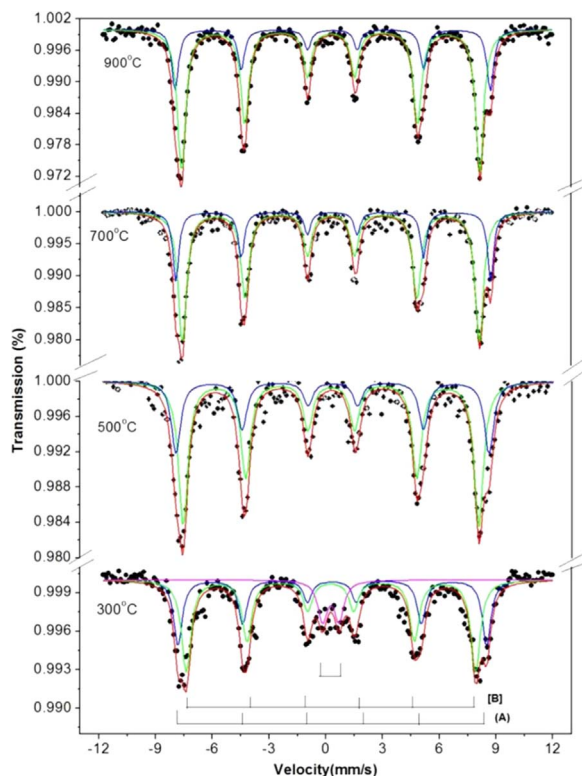


Fig. 5. Mössbauer spectra of CoFe_2O_4 sintered at different temperatures.

temperature $f_B/f_A=1$) which gives the Co^{+2} occupation at the A site and hence the deviation from the inverse spinel structure may be determined [29].

The Mössbauer parameters for CoFe_2O_4 particles having different sintering temperatures are given in Table 3. The characteristic range of isomer shift is often associated with particular oxidation state of Mössbauer atom. In this work isomer shift values are with respect to natural iron foil. The values of isomer shift (< 1 mm/s) indicates that the iron is in Fe^{+3} state. The sample sintered at 300 °C shows a clear

Table 3
Mössbauer parameters for the synthesized samples.

Sint. temp. (°C)	Site	IS (mm/s) ± 0.02	QS (mm/s)	Γ (mm/s)	B_{hf} (T)	% Area ± 0.05	Cation distribution	$M_B - M_A$ (μ_B)
300	A	0.25	0	0.54 ± 0.0	50.0 ± 0.16	34.77	$(\text{Co}_{0.21}\text{Fe}_{0.79})$ $[\text{Co}_{0.79}\text{Fe}_{1.21}]_0\text{O}_4$	4.30
	B	0.35	0	0.60 ± 0.0	47.7 ± 0.04	53.61		
	Para.	0.15	1.03 ± 0.04	0.60 ± 0.0	0	11.62		
500	A	0.39	0	0.58 ± 0.02	51.2 ± 0.06	32.80	$(\text{Co}_{0.35}\text{Fe}_{0.65})$ $[\text{Co}_{0.65}\text{Fe}_{1.35}]_0\text{O}_4$	4.64
	B	0.43	0	0.61 ± 0.03	48.3 ± 0.08	67.20		
700	A	0.37	0	0.39 ± 0.00	51.69 ± 0.09	28.15	$(\text{Co}_{0.43}\text{Fe}_{0.57})$ $[\text{Co}_{0.57}\text{Fe}_{1.43}]_0\text{O}_4$	4.85
	B	0.27	0	0.53 ± 0.01	48.79 ± 0.00	71.85		
900	A	0.47	0	0.41 ± 0.03	51.7 ± 0.05	27.25	$(\text{Co}_{0.55}\text{Fe}_{0.45})$ $[\text{Co}_{0.45}\text{Fe}_{1.55}]_0\text{O}_4$	5.12
	B	0.48	0	0.49 ± 0.16	48.4 ± 0.14	72.75		

Note: IS – isomer shift; QS – quadrupole splitting; Γ – Line width; B_{hf} – hyperfine field.

paramagnetic doublet along with two sextets (Fig. 5). It is suggested that this doublet may be arised due to superparamagnetic nature of smaller sized particles present in the sample [30]. The critical size of superparamagnetism is ~ 14 nm for CoFe_2O_4 [20–31]. Superparamagnetism is a characteristic feature of small crystallites where the magnetization is not fixed in any of the easy axes, and it is due to the magnetic spin fluctuation between the easy axes of magnetization when the external magnetic field is absent. The average time required for the change of magnetization from one easy axis to another is called superparamagnetic relaxation time (τ) and it depends on both crystallite size and the temperature. The value of $\tau = \tau_0 \exp(KV/k_B T)$ where K is the anisotropy constant of the crystallite, V crystallite volume, k_B the Boltzmann constant, T is the absolute temperature and τ_0 is a constant ($\sim 10^{-10}$ s) [18–31]. The characteristic flipping time of magnetization in superparamagnetic particles are smaller than the characteristic time of Mössbauer measurements ($\sim 5 \times 10^{-9}$ s) [32]. Therefore the Mössbauer nuclide does not see a net magnetization and thus there is no Zeeman splitting in smaller sized particles. At constant temperature, relaxation time depends only on the crystallite volume. As the sintering temperature increases paramagnetic phase vanishes because above 500 °C cobalt ferrite shows complete crystallization and particle size grows rapidly.

The value of magnetic moment per formula unit calculated by cation distribution (Neel's two sublattice model of ferrimagnetism) is not matching with the values found with the help of VSM (experimental values). This discrepancy may be due to the spin canting at B site. Spin canting is defined as a lack of full alignment of spins. The canting angle ϕ can be calculated using the following assumption

$$M = M_B \cos \phi - M_A$$

The calculated value of canting angle comes out to be ~ 39.81 , 32.44 , and 33.63 and 33.29° for the samples sintered at 300, 500, 700 and 900 °C respectively. Other workers have also reported the values of canting angle in the similar range [33]. However, for the direct verification of this canting, in field Mössbauer spectroscopy is planned.

The Mössbauer hyperfine parameters are listed in Table 3. Cation distribution shows that as the sintering temperature increases the cobalt concentration at the A site also increases. This indicates that the synthesized sample is trying to have the normal spinel structure at

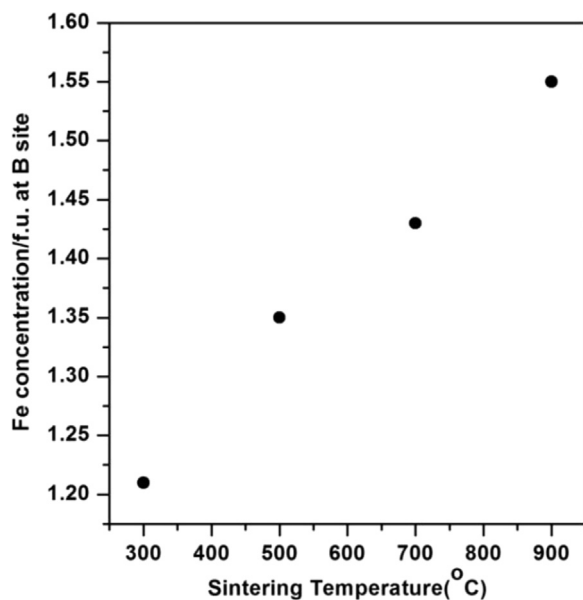


Fig. 6. Iron concentration at B site as a function of sintering temperature.

higher sintering temperatures. Fig. 6 shows that as the sintering temperature increases from 300 to 900 °C the iron concentration per formula unit at B site increases from 1.21 to 1.55. This may be responsible for the large value of saturation magnetization at higher sintering temperatures as evidenced by VSM. Some other workers studied the cation distribution in cobalt ferrite sintered at 1200 °C for $(\text{Co}_{0.40}\text{Fe}_{0.60})[\text{Co}_{0.60}\text{Fe}_{1.40}]\text{O}_4$ [34] prepared by aerosol method, which is similar to the cation distribution sintered at 700 °C in our study. It indicates that there may be some inversion temperature between 900 and 1200 °C at which the cobalt ferrite again starts to get the inverse spinel structure and Fe^{+3} start migrating from B site to A site as is the case of bulk cobalt ferrite [35].

4. Conclusions

In this work we report the effect of sintering temperature on different properties of cobalt ferrite nanoparticles prepared by sol-gel method. XRD results show the pure phase of cobalt ferrite. Particle size and lattice parameter values are in good agreement with the literature. The XRD patterns show that the crystalline nature is increasing with increase in sintering temperature. This effect is more dominant above 500 °C. Histogram plotted with the help of TEM image shows the particle size distribution is symmetric about ~25 nm. The selected area diffraction pattern shows the polycrystalline nature of the sample and rings are corresponding to the different planes. The VSM result indicates that the magnetic ordering in the system increases with the increase of sintering temperature. The value of saturation magnetization is increasing with sintering temperature which confirms that the magnetic moment of B site is increasing, indicating that there is migration of Fe^{+3} ions from A site to B site. Mössbauer spectroscopic analysis confirmed that all the samples are ferrimagnetic in nature. The spectral area ratio [B]/(A) site is consistently increasing with sintering temperature. This confirms that Fe^{+3} ions transfer from A site to B site. Thus the Mössbauer study supports the results of VSM. The calculated structural formula using Mössbauer technique shows that there is a direct effect of sintering temperature on cation distribution between A

and B sites. In view of the large value of saturation magnetization of the synthesized samples these are suitable for applications such as in high density information storage and ferrofluids technology.

Acknowledgements

Authors are thankful to Dr. Ajay Gupta and Dr. Alok Banerjee, UGC-DAE CSR, Indore Center (India) for providing the experimental facilities and fruitful discussion.

References

- [1] K. Praveena, K. Sadhana, S. Bharawaj, S.R. Murthy, J. Magn. Mater. 321 (2009) 2433.
- [2] H.M. Lu, W.T. Zheng, Q. Jiang, J. Phys. D: Appl. Phys. 40 (2007) 320–325.
- [3] R.M. Mohamed, M.M. Rashad, F.A. Haraz, W. Sigmund, J. Magn. Mater. 322 (2010) 2058–2064.
- [4] German Salazar-Alvarez, Richard T. Olsson Jordi Sort, Waldemar A.A. Macedo, Jose D. Ardisson, Maria Dolores Baro, Ulf W. Gedde, Josep Nogués, Chem. Mater. 19 (2007) 4957–4963.
- [5] J.G. Dos, S. Duque, M.A. Macedo, N.O. Moreno, J.L. Lopez, H.D. Pfanès, J. Magn. Mater. 1424 (2001) 226–230.
- [6] R.N. Panda, J.C. Shih, T.S. Chin, J. Magn. Mater. 257 (2003) 79–86.
- [7] S.D. Sartale, C.D. Lokhande, Ceram. Int. 28 (2002) 467.
- [8] C.H. Yan, Z.G. Xu, F.X. Cheng, Z.M. Wang, L.D. Sun, C.S. Liao, J.T. Jia, Solid State Commun. 111 (1999) 287.
- [9] M.I. Godinho, M.A. Catarino, M.I. da Silva Pereira, M.H. Mendonc, F.M. Costa, Electrochim. Acta 47 (2002) 4307.
- [10] R. Valenzuela, Magnetic Ceramics, Cambridge University Press, Cambridge, 1994.
- [11] P. Chandramohan, M.P. Srinivasan, S. Velmurugan, S.V. Narasimhan, J. Solid State Chem. 184 (2011) 89–96.
- [12] Lanhong Ai, Jing Jiang, Curr. Appl. Phys. 10 (2010) 284–288.
- [13] K.H.J. BUSCHOW, J. Less-Common Met. 155 (1989) 307–318.
- [14] Sonal Singhal, Tsering Namgyal, Sandeep Bansal, Kailash Chandra, J. Electromagn. Anal. 2 (2010) 376–381.
- [15] Jitendra Pal Singh, R.C. Srivastava, H.M. Agrawal, Ravi Kumar, V.R. Reddy, Ajay Gupta, J. Magn. Mater. 322 (2010) 1701–1705.
- [16] B.D. Cullity, Elements of X-Ray Diffraction, Addison-Wesley, New York, 1972.
- [17] C.O. Augustin, L.K. Srinivasan, P. Kamraj, A. Mani, J. Mater. Sci. Technol. 12 (1996) 417–420.
- [18] Kula K. Senapati, C. Borgohain, P. Phukan, J. Mol. Catal. A: Chem. 339 (2011) 24–31.
- [19] Sandeep Kohli, Patrick R. Mc Curdy, Derek C. Johnson, Jaydip Das, Amy L. Prieto, Christopher D. Rithner, Ellen R. Fisher, J. Phys. Chem. C 114 (2010) 19557–19561.
- [20] G.S. Rajana, S.L. Stromeyera, K.A. Mauritz, G. Miaob, P. Manib, M. Shamsuzzohab, David E. Niklesb, A. Gupta, J. Magn. Mater. 299 (2006) 211–218.
- [21] Richard J. Harrison, Andrew Putnis, Am. Mineral. 80 (1995) 213–221.
- [22] Suman, N.D. Sharma, Indian J. Pure Appl. Phys. 15 (2007) 549–554.
- [23] Yasuhiro Konishi, Toshiyuki Nomura, Kazunari Mizoe, Kazutaka Nakata, Mater. Trans. 45 (1) (2004) 81–85.
- [24] L. Ben Tahar, M. Artus, S. Ammar, L.M. Smiri, F. Herbst, M.J. Vaulay, V. Richard, M. Greneche, F. Villain, F. Fievet, J. Magn. Mater. 320 (2008) 3242.
- [25] J.L. Slonczewski, Phys. Rev. 110 (1958) 1341.
- [26] B.D. Cullity, Introduction to Magnetic Materials, Addison-Wesley, New York, 1972.
- [27] Shun Hua Xiao, Wei Fen Jiang, Long Yu Li, Xin Jian Li, Mat. Chem. Phys. 106 (2007) 82–87.
- [28] R.A. Brand, Normos Mossbauer fitting program, Nucl. Instrum. Methods B28 (1987) 398.
- [29] V. Rusanav, V. Gushterov, S. Nikolov, A.X. Trautwein, Hyperfine Inter. 191 (2009) 67–74.
- [30] Jae-Gwang lee, Jae Yun Park, Chul Sung Kim, J. Mater. Sci. 33 (1998) 3965–3968.
- [31] R. Sani, A. Beitollahi, Yu.V. Maksimov, I.P. Suzdalev, J. Mater. Sci. 42 (2007) 2126–2131.
- [32] G.F. Goya, H.R. Rechenberg, J.Z. Jiang, J. Appl. Phys. 84 (2) (1998).
- [33] V. Sepelak, D. Baabe, F.J. Litterst, K.D. Becker, J. Appl. Phys. 88 (10) (2000).
- [34] Sonal Singhal, S.K. Brthwal, K. Chandra, J. Magn. Mater. 306 (2006) 233–240.
- [35] Pham D. Thang, Guus Rijnders, Dave H.A. Blank, J. Magn. Mater. 295 (2005) 251–256.